

# VidPrism: Heterogeneous Mixture of Experts for Image-to-Video Transfer

Rui Lin Chuanming Wang Huadong Ma\*  
 State Key Laboratory of Networking and Switching Technology,  
 Beijing University of Posts and Telecommunications, China  
 {lr\_507, wcm, mhd}@bupt.edu.cn

## Abstract

With the rapid development of pre-training technologies, adapting large-scale Vision-Language Models (VLMs) for video understanding i.e. image-to-video transfer learning has become a dominant paradigm. To achieve superior performance, it raises as an effective strategy among recent advances to employ Mixture-of-Experts (MoE) to enhance VLMs’ temporal modeling capabilities. However, conventional MoE designs suffer from expert homogenization, where all experts act as identical generalists, inefficiently learning spatio-temporal features from undifferentiated video streams. To overcome this problem, we propose VidPrism, a novel heterogeneous temporal Mixture-of-Experts framework. VidPrism pioneers a division of labor by deploying functionally specialized experts, each assuming a role ranging from spatial understanding to temporal modeling. To feed these specialists appropriately, we introduce a content-aware, multi-rate sampling module that dynamically generates streams ranging from semantically rich to motion-focused representations, providing specialized inputs for experts. Furthermore, a dynamic, bidirectional fusion mechanism enables synergistic information exchange between these pathways, leading to a comprehensive video representation. Extensive experiments on various video recognition benchmarks demonstrate that VidPrism achieves state-of-the-art performance and effectively fosters expert specialization. Our source code is available at <https://github.com/Lrrrr549/VidPrism.git>.

## 1. Introduction

The emergence of large-scale fundamental models has driven a paradigm shift in the field of artificial intelligence, where Visual Language Models (VLMs) [26, 42, 46] are at the forefront of this revolution. These models are pre-trained on massive image-text pair datasets and demonstrate superior few-shot learning capabilities in a variety of down-

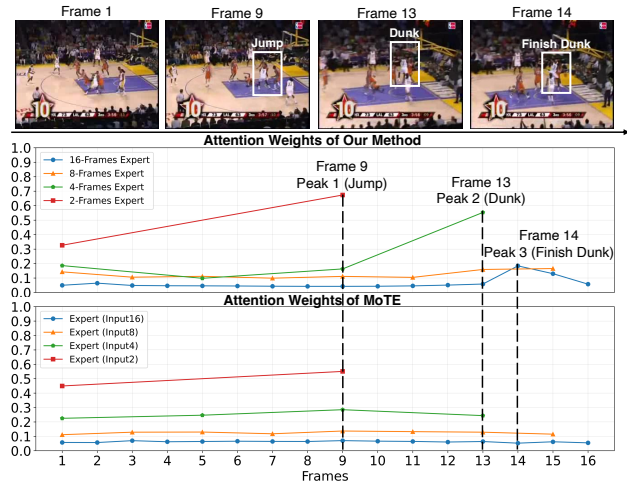


Figure 1. **Visualization of inter-frame attention distribution.** We select a video from the Dunk category in UCF-101 [30] to compare inter-frame attention between MoTE and our method. Using the same four-frame configurations for fairness, our model exhibits clear attention peaks at key moments, while the homogeneous MoTE baseline shows flat, indistinct distributions.

stream vision tasks. Therefore, significant performance improvements have been achieved in few-shot image analysis [3, 13]. However, compared to images, video data exhibits stronger continuity and temporal relevance, and the widely used image pre-training process results in video language models lacking the ability to handle temporal relevance. This weakens their performance in video understanding, which has been more widely used in real-world applications.

Consequently, how to adapt these VLMs to the domain of video understanding (i.e. Image-to-Video (I2V) transfer learning) has become one of the core issues in current research. Among recent advance works, adding additional temporal modules [6, 23, 45] to explicitly model of temporal dynamics has attracted increasing attention due to its flexibility and strong performance, and some works have begun to explore the introduction of Mixture-of-Experts (MoE) architecture as such temporal modules [54].

\*Corresponding author: Huadong Ma

Nevertheless, traditional MoE designs face an inherent limitation when applied to complex and multifaceted data such as video: expert homogenization. In standard MoE, all experts are trained using the same undifferentiated input stream. This forces each expert to become a generalist, redundantly learning overlapping features. This design is inefficient for video because it fails to create specialized computational paths to model inherently different types of information, such as the static content of a scene and its temporal evolution. The limitation is verified in Figure 1. The baseline MoTE [54] method exhibits flat and diffused attention, failing to identify critical moments in the action.

This problem raises us a question intuitively, can we process the video frames by a group of heterogeneous experts, each operating at different perspectives. This insight also conforms to the core concept in *two-stream hypothesis* of neuroscience [11], which posits parallel ‘what’(spatial) and ‘how’(temporal) pathways in the brain to understand complex video contents. However, constructing such a heterogeneous multipath architecture still faces two key challenges: 1. How to provide the most relevant input to each expert? 2. How can these experts achieve effective collaboration and information sharing?

To address these challenges, we first extend this concept of the two-stream hypothesis from a fixed dual-pathway architecture to a more flexible multipathway framework, and develop a novel heterogeneous temporal MoE framework called VidPrism. VidPrism enables specialized processing of information at different temporal scales by dynamically generating specialized multi-rate input streams and binding them to heterogeneous expert networks. It incorporates a group of spatial-temporal experts focusing on different spatial-temporal resolutions, thereby achieving greater knowledge capacity and finer specialization within each functional domain.

To provide specialized input for experts (challenge 1), VidPrism introduces a content-aware mechanism that splits the input video into multiple distinct multi-rate streams. The low-rate stream captures keyframes with rich semantic context and routes them to the expert group responsible for spatial reasoning. Simultaneously, the high-rate stream focuses on high-frequency temporal variations and directs them to the expert group specifically responsible for motion modeling. To facilitate collaboration and information exchange among experts (challenge 2), we design a bidirectional fusion module, which helps the model to build a holistic understanding of the video by integrating global scene context and complex temporal dynamics. Finally, the outputs of all experts are aggregated to form a unified video-level representation for classification. VidPrism allows for a dynamic division of labor among functionally heterogeneous experts, enabling the model to focus on critical action moments, as validated in Figure 1.

Our main contributions can be summarized as follows:

- We are the first to propose a heterogeneous Mixture-of-Experts architecture for image-to-video transfer, where expert networks are explicitly specialized and bound to different temporal scales.
- We design a content-aware multi-rate input generation module that dynamically generates semantically rich slow-rate streams and motion-dense fast-rate streams, providing specialized input for different experts.
- We introduce a dynamic, bidirectional fusion mechanism that enables synergistic information exchange between the spatial and temporal expert pathways.

## 2. Related Work

**Video Recognition.** Early video recognition relied on handcrafted features [34], combined appearance and motion via optical flow. Two-Stream Networks [9, 29] processed RGB frames and optical flow separately to model motion explicitly. 3D CNNs [5, 14, 18, 32, 36] learned spatio-temporal representations directly from raw pixels through spatial-temporal convolutions, reducing dependence on pre-computed motion. Transformer-based models [1, 4, 8, 19, 21, 23, 52] treated videos as sequences of spatio-temporal patches, using self-attention to capture long-range dependencies beyond CNNs’ local receptive fields. Recently, multimodal large models [31, 33, 43, 50] integrate visual and textual modalities into unified representations, advancing video understanding abilities.

**I2V Transfer Learning.** Adapting pre-trained image foundation models, particularly VLMs [26, 42, 46], for video recognition has become a prevalent and parameter-efficient paradigm. To bridge the domain gap from static images to dynamic videos, early work augmented frozen image encoders with simple temporal pooling. More sophisticated approaches followed, introducing lightweight, trainable modules like temporal adapters [19, 24] and embeddings [23, 38] to explicitly model temporal dependencies. This trend has evolved towards more intricate structural modifications, including learnable queries [40] and advanced spatio-temporal adapters [6].

**Multi-Pathway Temporal Modeling.** Multi-pathway architectures [10] employ dual-rate pathways to capture slow spatial semantics and fast motion, inspiring a range of spatial-temporal decomposition strategies [5, 18, 32] and feature-level hierarchies [16, 41, 51]. Extensions to multimodal large language models [22, 28, 35, 47, 48] have further shown the promise of multi-path designs for long-range and fine-grained reasoning. Furthermore, approaches employing Mixture-of-Experts (MoE) frameworks for temporal modeling [54] introduce conditional expert routing to enhance temporal specialization. Yet, most existing multi-path methods operate at fixed, preset frame rates. This static design limits adaptability. In contrast, our het-

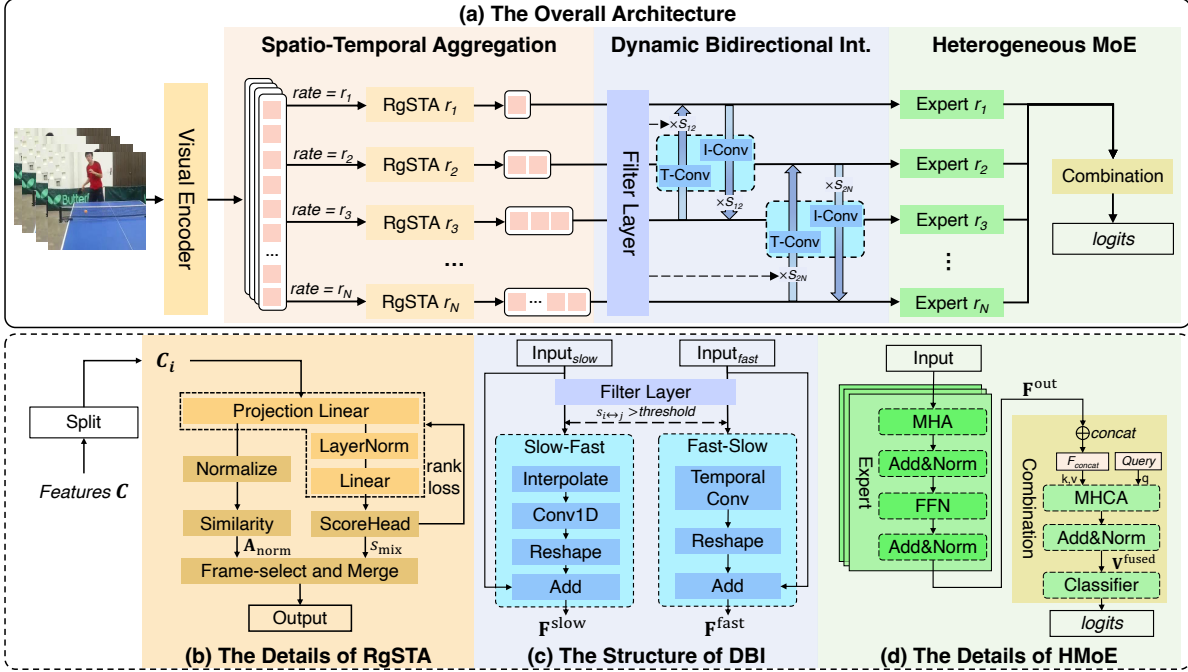


Figure 2. An overview of VidPrism: (1) A visual encoder processes the input video to extract a sequence of frame-level features. (2) Multiple RgSTA modules then tokenize these features into  $N$  parallel streams, each with a distinct spatio-temporal resolution. (3) The DBI module facilitates selective information fusion across the multi-rate streams. (4) HMoE models each enriched stream and integrates outputs into a comprehensive global representation for final classification.

erogeneous MoE dynamically associates specialized experts with content-adaptive, multi-rate inputs, enabling fine-grained collaboration across temporal scales.

### 3. Method

The overview of our method is shown in Figure 2. Next, we will introduce the specific design of VidPrism in detail.

#### 3.1. Diverse Spatio-Temporal Aggregation

Given an input video, we first send it to a visual encoder to extract frame-level features  $\mathbf{C} \in \mathbb{R}^{T \times B \times D}$ , where  $T$ ,  $B$ , and  $D$  denote the number of frames, batch size, and feature dimension, respectively. Since input video usually contains redundant information, spatial-temporal aggregation should be performed to produce compact and robust representations. Traditional strategy samples frame features at a fixed rate, which may cause the overlook of important temporal information. Thus, we propose a diverse spatio-temporal aggregation method, in which frame features are sampled at different rates and processed by specialized pathways.

The core designed module in the aggregation step is Rate-guided Spatio-Temporal Aggregation Module (RgSTA), where rate stands for different spatio-temporal resolutions, aiming at efficiently fusing temporal features while maximising the retention of critical dynamic spatio-temporal information by merging rather than discarding information. The details of STA is shown in the Figure 2(b).

After splitting the frame features  $\mathbf{C}$  according to the rate  $r_i$  into  $\mathbf{c}_i \in \mathbb{R}^{T_i \times B \times D}$ , where  $T_i = T/r_i$  denotes the temporal length of the  $i$ -th pathway, RgSTA first assesses the importance of each frame feature, and a hybrid scoring mechanism is introduced, which will combine learnable importance scores  $s_{\text{pred}}$  and the intrinsic properties  $s_{\text{norm}}$  of the features themselves, aiming to achieve a more comprehensive frame importance evaluation.

For the scores  $s_{\text{pred}}$ , we introduce a score head to predict the importance of each feature. Specifically, the input feature  $\mathbf{c}_i$  is first projected into a metric space, and then a scalar score is obtained through the scoring header. The process can be formulated as:

$$s_{\text{pred},i} = \text{ScoreHead}(\text{LN}(\text{MetricProj}(\mathbf{c}_i))), \quad (1)$$

where LN means LayerNorm[2]. Both MetricProj and ScoreHead are implemented by a linear layer. This design allows the model to autonomously learn to determine which features are critical based on task goals.

For the intrinsic properties  $s_{\text{norm}}$ , we are of the view that the L2 norm of a feature can reflect its intrinsic importance to some extent, i.e., features with larger paradigms usually contain richer signals [49, 53]. Therefore, we compute the L2 norm of each feature as its intrinsic score  $s_{\text{norm},i} = \|\mathbf{c}_i\|_2$ . The final importance score  $s_{\text{mix}}$  is a weighted fusion of the above two outputs:

$$s_{\text{mix},i} = \alpha \cdot s_{\text{pred},i} + (1 - \alpha) \cdot s_{\text{norm},i} \quad (2)$$

where  $\alpha \in [0, 1]$  is a hyperparameter used to balance the importance between  $s_{\text{pred}}$  and  $s_{\text{norm}}$ .

Within each group, we select a feature with the highest score  $s_{\text{mix}}$  to form a kept set, while the remaining features constitute a rest set. To avoid discarding the information of the rest set, we design a fusion mechanism. We compute the cosine similarity between features in the rest set  $\mathbf{C}_{\text{rest}} \in \mathbb{R}^{1 \times B \times D}$  and the kept set  $\mathbf{C}_{\text{kept}} \in \mathbb{R}^{(T_i-1) \times B \times D}$  to obtain a similarity matrix  $\mathbf{S}_{\text{rest} \rightarrow \text{kept}} \in \mathbb{R}^{(T_i-1) \times 1 \times B}$ .

This matrix is then normalized by a Softmax function to yield the weight matrix  $\mathbf{A}_{\text{norm}}$ :

$$\mathbf{Z}_{\text{kept}} = \text{Norm}(\text{MetricProj}(\mathbf{C}_{\text{kept}})), \quad (3)$$

$$\mathbf{Z}_{\text{rest}} = \text{Norm}(\text{MetricProj}(\mathbf{C}_{\text{rest}})), \quad (4)$$

$$\mathbf{S}_{\text{rest} \rightarrow \text{kept}} = \mathbf{Z}_{\text{rest}} \mathbf{Z}_{\text{kept}}^T, \quad (5)$$

$$\mathbf{A}_{\text{norm}} = \text{Softmax}\left(\frac{\mathbf{S}_{\text{rest} \rightarrow \text{kept}}}{\tau}\right), \quad (6)$$

where  $\tau$  is the temperature coefficient. For each feature in the rest set, its information is distributed to the kept set based on these attention weights. Specifically, the information from the rest set is accumulated into the kept set by a weighted summation:

$$\mathbf{C}'_{\text{kept}} = \mathbf{C}_{\text{kept}} + \delta(\mathbf{A}_{\text{norm}})^T \mathbf{C}_{\text{rest}}, \quad (7)$$

where  $\delta$  is a scaling factor to moderate the magnitude of the update. The feature  $\mathbf{F} \in \mathbf{C}'_{\text{kept}}$  generated by each RgSTA subsequently enter parallel processing pathways.

This approach yields two benefits. On the one hand, it makes the sequence more compact by selecting only the most important frames. On the other hand, instead of discarding information from the dropped frames, it integrates features into the selected keyframes. This process enriches the keyframes, ensuring that no valuable information is lost while making the representation more efficient.

### 3.2. Dynamic Bidirectional Interaction

In VidPrism, different pathways capture the dynamic information of video at different temporal resolutions. To enable these specialised pathways to collaborate rather than operate in isolation, we propose to adopt a dynamic bidirectional interaction scheme to exchange information among these pathways. According to Figure 2(c), by employing a filter mechanism, selective bidirectional information is exchanged by the designed Dynamic Bidirectional Interaction (DBI) module.

To determine the necessity and strength of information exchange between any two pathways  $i$  and  $j$ , we design a lightweight filter network  $\mathcal{G}_{i \leftrightarrow j}$  for each pair of pathways  $(i, j)$ . This network dynamically generates an interaction score  $s_{i \leftrightarrow j} \in [0, 1]$  based on the global context information of the two pathways.

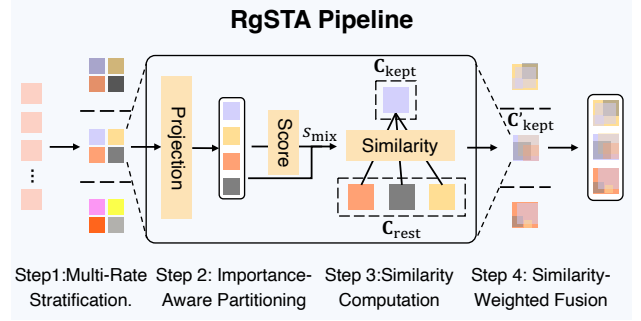


Figure 3. A pipeline of STAM: (1) Input features are stratified into groups. (2) Within each group, an importance score divides the features into kept and rest sets. (3) Pairwise similarity between the two sets is computed to generate attention weights. (4) Ultimately, the features in the rest set are aggregated back to the kept set by attentional weighted summation.

Specifically, given  $\mathbf{F}_i \in \mathbb{R}^{T_i \times D}$  for the  $i$ -th pathway and  $\mathbf{F}_j \in \mathbb{R}^{T_j \times D}$  for the  $j$ -th pathway, we first extract the respective global summary vectors  $\mathbf{g}_i$  and  $\mathbf{g}_j$  by time dimensional global average pooling. These two vectors are then spliced and fed into a proprietary MLP, which is activated by a Sigmoid function to obtain the interaction score:

$$\mathbf{g}_k = \frac{1}{T_k} \sum_{t=1}^{T_k} \mathbf{F}_k, \quad k \in \{i, j\} \quad (8)$$

$$s_{i \leftrightarrow j} = \sigma(\text{MLP}_{i \leftrightarrow j}([\mathbf{g}_i; \mathbf{g}_j])), \quad (9)$$

where  $[\cdot; \cdot]$  denotes a vector splice and  $\sigma$  is a Sigmoid function.  $s_{i \leftrightarrow j}$  acts as a gate score that dynamically regulates the amount of information flowing between pathways  $i$  and  $j$ . To improve computational efficiency and promote sparse connectivity, we set a threshold. When  $s_{i \leftrightarrow j}$  meets the threshold, the bidirectional interaction is conducted by DBI modules. DBI is performed on two different-rate pathways, so it supports two complementary streams: a Slow-to-Fast information flow providing high-level context, and a Fast-to-Slow information flow delivering rich temporal details.

**Slow-to-Fast Path.** When information needs to be passed from the slow pathway to the fast pathway, the alignment of the temporal and channel dimensions must be addressed. We first use linear interpolation  $\mathbf{I}$  to upsample the temporal dimension  $T_i$  of the slow pathway feature  $\mathbf{F}_i$  to align with the temporal dimension  $T_j$  of the fast pathway feature  $\mathbf{F}_j$  to obtain  $\mathbf{F}'_i$ . The  $\mathbf{F}'_i$  is then passed through a  $1 \times 1$  convolutional layer for channel adaptation and feature transformation. The transformed features are then multiplied by a dynamically gated fraction  $s_{i \leftrightarrow j}$  and added to the original features  $\mathbf{F}_j$  of the fast pathway in a residual-join fashion. This can be formulated as:

$$\mathbf{F}_j^{\text{fast}} = \mathbf{F}_j + s_{i \leftrightarrow j} \cdot \text{Conv}_{1 \times 1}(\mathbf{I}(\mathbf{F}_i)). \quad (10)$$

**Fast-to-Slow Path.** When information flows from the

fast to the slow pathway, then temporal downsampling is required. We apply a temporal convolution with a step size of  $S = R_j/R_i$  to the fast pathway feature  $\mathbf{F}_i$ , where  $R_i$  and  $R_j$  are the temporal sampling rates of pathways  $i$  and  $j$ , respectively. This operation reduces the temporal resolution while effectively aggregating dynamic information within a local time window. The convolved features are similarly multiplied by the corresponding gating scores  $s_{i \leftrightarrow j}$ , added to the slow pathway features  $\mathbf{F}_j$ :

$$\mathbf{F}_j^{\text{slow}} = \mathbf{F}_j + s_{i \leftrightarrow j} \cdot \text{T-Conv}(\mathbf{F}_i). \quad (11)$$

In this way, information about movement changes captured by the fast pathway can be refined and injected into the slow pathway, thus enriching its understanding of the overall structure of the movement. When one-to-multi information exchange occurs, we process raw features from all paths in parallel, weight them by their gating scores, and accumulate the aggregated information into the target path.

### 3.3. Heterogeneous Mixture-of-Experts

The spatio-temporal features processed by 3.1 and 3.2 possess differing lengths and semantic focus. To better capture the information within them and integrate them into a globally unified video representation, as shown in Figure 2(d), we design a Heterogeneous Mixture-of-Experts (HMoE) module comprising a set of heterogeneous experts and a combination block.

**Heterogeneous Experts.** Each input feature corresponds to a separate expert module. These expert modules are designed to learn and model the internal temporal dependencies at the corresponding time scales, thereby achieving functional heterogeneity. Each expert is designed as a standard Transformer layer and is exclusively trained on a single, specific temporal rate. Given an input sequence  $\mathbf{F}_i \in \mathbb{R}^{T_i \times D}$ , the processing flow is as follows:

$$\mathbf{F}'_i = \text{LN}(\mathbf{F}_i + \text{MHSA}(\mathbf{F}_i)), \quad (12)$$

$$\mathbf{F}_i^{\text{out}} = \text{LN}(\mathbf{F}'_i + \text{FFN}(\mathbf{F}'_i)). \quad (13)$$

Among them, MHSA refers to Multi-Head Self-Attention, FFN is a feed-forward network containing two linear layers and a GELU activation function.

**Combination Mechanism.** After experts process their respective sequences independently, a combination module is adopted to aggregate this diverse information. The module introduces a learnable global query vector that makes it traverse the outputs of all experts and extracts the comprehensive information that is most important for the task.

We splice the output sequences  $\mathbf{F}_1^{\text{out}}, \dots, \mathbf{F}_N^{\text{out}}$  of all the  $N$  experts in the time dimension to obtain  $\mathbf{F}_{\text{concat}} \in \mathbb{R}^{(\sum T_i) \times D}$ . Also, we introduce a learnable global query parameter  $\mathbf{q}_{\text{global}} \in \mathbb{R}^{1 \times D}$ , whose task is to learn how to efficiently summarise information from  $\mathbf{F}_{\text{concat}}$  during training. We perform a multi-headed cross-attention operation

with  $\mathbf{q}_{\text{global}}$  as the Query and  $\mathbf{F}_{\text{concat}}$  as the Key and Value:

$$\mathbf{V}_{\text{fused}} = \text{MHA}(\mathbf{q}_{\text{global}}, \mathbf{F}_{\text{concat}}), \quad (14)$$

$$\text{logits} = \text{Classifier}(\mathbf{V}_{\text{fused}}), \quad (15)$$

where MHA is Multi-Head Attention. The output of this operation  $\mathbf{V}_{\text{fused}} \in \mathbb{R}^{1 \times D}$  is a single vector representing a weighted aggregation of all experts' features, with the weights determined dynamically by the similarity of the query vector to the individual features. Finally,  $\mathbf{V}_{\text{fused}}$  passes through a classifier to produce classification logits.

### 3.4. Training Objectives

To monitor the learning process of the VidPrism, we employ four loss functions.

**Classification Loss.** We employ the standard classification cross-entropy loss  $\mathcal{L}_{\text{cls}}$ , applied to the final fused feature vector  $\mathbf{v}_{\text{fused}}$ . This loss serves as the primary guidance for the network's overall learning.

$$\mathcal{L}_{\text{cls}} = -\frac{1}{N} \sum_{i=1}^N \sum_{c=1}^C y_{i,c} \log(\text{softmax}(\text{logits}_{i,c})), \quad (16)$$

where  $N$  is the batch size,  $C$  is the number of classes,  $y_{i,c}$  is the one-hot ground-truth label, and  $\text{logits}_{i,c}$  is the predicted score for class  $c$  of the  $i$ -th sample.

**Ranking Loss.** To guide the ScoreHead module (in 3.1) towards learning more reliable importance rankings, we introduce an auxiliary ranking loss. This loss aims to make the distribution of predicted scores  $s_{\text{pred}}$  approximate the distribution of target scores  $s_{\text{tgt}}$ .  $s_{\text{tgt}}$  is computed by combining feature norm and average similarity within its window:

$$s_{\text{tgt},i} = \|\mathbf{c}_i\|_2 + \frac{1}{N} \sum_{j=1}^N \mathbf{S}_{ij}. \quad (17)$$

We employ the Kullback-Leibler divergence to measure the difference between these two score distributions, defining it as the ranking loss  $\mathcal{L}_{\text{rank}}$ :

$$\mathcal{L}_{\text{rank}} = \text{KL}(\text{Softmax}(s_{\text{tgt}}/T_s) \parallel \text{Softmax}(s_{\text{pred}}/T_s)), \quad (18)$$

where  $T_s$  is a temperature hyperparameter.

**Diversity Loss.** Concurrently, to encourage experts to learn complementary features, we introduce the diversity loss  $\mathcal{L}_{\text{div}}$ . This loss aims to maximise the distance between feature outputs from different experts. Specifically, it computes the cosine similarity between output features  $\bar{\mathbf{F}}_i^{\text{out}}$  and  $\bar{\mathbf{F}}_j^{\text{out}}$  for each expert pair  $(i, j)$ :

$$\mathcal{L}_{\text{div}} = \frac{1}{\binom{N}{2}} \sum_{i < j} \text{D}(\bar{\mathbf{F}}_i^{\text{out}}, \bar{\mathbf{F}}_j^{\text{out}}). \quad (19)$$

By minimising this loss, we incentivise each expert to focus on capturing dynamic information at its unique temporal scale, thereby enhancing the representational capability of the entire hybrid expert system.

**Gate Balancing Loss.** To prevent the Readout module from over-relying on a minority of experts during fusion while neglecting others’ contributions, we introduce the gating balancing loss  $\mathcal{L}_{\text{gate}}$ . Given the gated weight matrix  $\mathbf{W} \in \mathbb{R}^{B \times N}$  produced by the Readout module’s attention, the balancing loss is defined as:

$$C_i = \frac{1}{B} \sum_{b=1}^B W_{b,i}, \quad (20)$$

$$\mathcal{L}_{\text{gate}} = N \cdot \sum_{i=1}^N C_i^2, \quad (21)$$

where  $W_{b,i}$  is expert  $i$ ’s contribution to sample  $b$ , and  $C_i$  is each expert’s average contribution within the batch. This loss takes effect by penalising imbalanced contributions.

The model’s overall loss function is a weighted sum of the aforementioned losses, defined as follows:

$$\mathcal{L}_{\text{total}} = \mathcal{L}_{\text{cls}} + \lambda_{\text{rank}} \mathcal{L}_{\text{rank}} + \lambda_{\text{div}} \mathcal{L}_{\text{div}} + \lambda_{\text{gate}} \mathcal{L}_{\text{gate}} \quad (22)$$

where  $\lambda_{\text{rank}}$ ,  $\lambda_{\text{div}}$ , and  $\lambda_{\text{gate}}$  are hyperparameters used to balance the contributions of each loss component.

## 4. Experiments

### 4.1. Experimental Setup

We conduct experiments on four video benchmarks: Kinetics-400 [5], UCF-101 [30], HMDB-51 [17] and SomethingSomething V2 (SSv2) [12]. Our research involves few-shot and fully-supervised video recognition. We use CLIP [26] with ViT-B/16 and ViT-L/14 as the visual backbone. The sparse frame sampling strategy for the video uses 8 and 32 frames during training and inference. For 8-frame sampling, we choose a triple expert with rates of 2,4,8; for 32-frame sampling, we use a quadruple expert architecture with rates of 2,4,8,16. All experiments are conducted on two NVIDIA A100 GPUs.

### 4.2. Main Results

**Close-set Results.** Table 1 shows the results of the comparison between VidPrism and the current video model of SOTA on the K400 dataset. We can first observe that our proposed VidPrism framework demonstrates significant performance benefits over the MoTE baseline, achieving a 1.0% accuracy improvement with a ViT-B/16 backbone and 8-frame input. This improvement persists with the ViT-L/14 backbone, maintaining a 0.6% advantage while requiring nearly identical computational resources. These results provide strong evidence that setting up dedicated timing experts is a more effective and efficient strategy for video representation learning. Second, using an 8-frame input with a ViT-B/16 backbone, VidPrism delivers 84.0% accuracy, nearly identical to the 84.1% from FocusVideo. Notably,

Table 1. Performance comparison on K400. Per-view GFLOPs are reported. Inputs mean frames×crops×clips.

Method	Inputs	Top-1 (%)	Top-5 (%)	GFLOPs
Adapting				
ST-Adapter-B/16 [24]	8×1×3	82.0	95.7	148
ST-Adapter-B/16 [24]	32×1×3	82.7	96.2	607
AIM-B/16 [52]	8×1×3	83.9	96.3	202
ActionCLIP-B/16 [38]	32×10×3	83.8	96.2	563
X-CLIP-B/16 [23]	8×4×3	83.8	96.7	145
Vita-CLIP-B/16 [44]	16×4×3	82.9	96.3	190
STAN-conv-B/16 [20]	8×1×3	83.1	96.0	238
M <sup>2</sup> -CLIP-B/16 [39]	8×4×3	83.4	96.3	214
M <sup>2</sup> -CLIP-B/16 [39]	32×4×3	84.1	96.8	842
ETL-ViCLIP-B/16 [6]	8×4×3	82.2	96.2	–
FocusVideo-B/16 [40]	8×4×3	84.1	96.5	204
FocusVideo-B/16 [40]	32×4×3	84.7	96.8	816
Tuning				
MoTE-B/16 [54]	8×4×3	83.0	96.3	141
Ost-B/16 [7]	16×1×1	83.2	–	–
VidPrism-B/16	8×4×3	84.0	96.8	162
VidPrism-B/16	32×4×3	<b>85.1</b>	<b>97.0</b>	721
Adapting				
ST-Adapter-L/14 [24]	8×1×3	86.7	97.5	687
ST-Adapter-L/14 [24]	32×1×3	87.2	97.6	2749
AIM-L/14 [52]	8×1×3	86.8	97.2	934
DUALPATH-L/14 [25]	32×1×3	87.7	97.8	–
M <sup>2</sup> -CLIP-L/14 [39]	32×4×3	87.0	97.6	–
FocusVideo-L/14 [40]	8×4×3	87.2	97.7	914
FocusVideo-L/14 [40]	32×4×3	88.0	<b>97.9</b>	3656
Tuning				
Text4Vis-L/14 [45]	32×4×3	87.1	97.4	1662
MoTE-L/14 [54]	8×4×3	86.8	97.5	649
MoTE-L/14 [54]	16×4×3	87.2	97.7	1299
VidPrism-L/14	8×4×3	87.4	97.8	632
VidPrism-L/14	32×4×3	<b>88.6</b>	<b>97.9</b>	2594

our method operates at a much lower computational cost, consuming just 162 GFLOPs while FocusVideo demands 204 GFLOPs. Furthermore, when the input is extended to 32 frames, VidPrism achieves a Top-1 accuracy of 85.1%, outperforming state-of-the-art methods such as MoTE and FocusVideo. This demonstrates that VidPrism achieves an excellent performance-efficiency balance, proving the effectiveness of our heterogeneous MoE architecture. When using the larger ViT-L/14 architecture, VidPrism achieves further performance gains, proving its scalability and viability in larger architectures. The above results demonstrate VidPrism’s efficiency and robustness in K400 video tasks.

**Few-shot video recognition.** Table 2 provides the evaluation of our method on the few-shot video recognition task. In few-shot experiments, in addition to the original CLIP, we additionally used VideoMAEv2 as the visual backbone to test the scalability of our architecture across different visual backbones. The model based on CLIP is called

Table 2. Performance comparison with state-of-the-art methods on HMDB51, UCF101 and SSv2 under various  $K$ -shot settings. In particular, the visual backbone of VidPrism-C is CLIP, while VidPrism-M uses VideoMAEv2.

Method	HMDB51				UCF101				SSv2			
	$K=2$	$K=4$	$K=8$	$K=16$	$K=2$	$K=4$	$K=8$	$K=16$	$K=2$	$K=4$	$K=8$	$K=16$
Zero-shot												
CLIP [26]	37.2	37.2	37.2	37.2	62.8	62.8	62.8	62.8	2.8	2.8	2.8	2.8
ViCLIP [42]	47.8	47.8	47.8	47.8	71.0	71.0	71.0	71.0	5.1	5.1	5.1	5.1
Adapting												
A5 [15]	39.7	50.7	56.0	62.4	71.4	79.9	85.7	89.9	4.4	5.1	6.1	9.7
X-CLIP [23]	53.0	57.3	62.8	64.0	76.4	83.4	88.3	91.4	3.9	4.5	6.8	10.6
ActionCLIP [38]	47.5	57.9	57.7	63.2	70.0	71.5	73.0	91.4	4.4	5.3	8.4	11.1
ViFi-CLIP [27]	57.2	62.7	64.5	66.8	80.7	85.1	90.0	92.7	6.2	7.4	8.5	12.4
ETL [6]	61.2	62.3	67.1	70.4	86.1	90.2	92.7	94.8	<b>9.1</b>	<b>10.4</b>	13.4	17.5
Tuning												
MAXI [27]	58.0	60.1	65.0	66.5	86.8	89.3	92.4	93.5	7.3	7.4	8.4	12.4
VideoMAEv2 [37]	38.6	52.3	63.2	72.2	73.4	86.8	92.1	94.7	5.0	8.6	12.2	17.1
OST [7]	60.0	62.5	65.6	67.3	83.0	88.4	91.3	93.9	7.3	8.4	8.5	11.5
MoTE [54]	<b>61.3</b>	63.9	67.2	68.2	88.8	91.0	92.3	93.6	7.3	8.5	9.5	12.2
ViCLIP [42]	53.7	60.4	64.5	70.3	83.0	88.0	92.1	93.2	8.7	9.7	11.6	15.4
VidPrism-C	55.0	<b>64.1</b>	<b>67.6</b>	<b>74.1</b>	88.1	<b>91.6</b>	<b>93.8</b>	<b>96.0</b>	4.9	7.3	9.3	14.1
VidPrism-M	53.4	63.3	<b>68.3</b>	<b>73.2</b>	<b>94.3</b>	<b>95.6</b>	<b>95.9</b>	<b>96.6</b>	6.4	9.5	<b>13.6</b>	<b>18.3</b>

Table 3. Ablation study on Number of Experts.

Experts Numbers	Experts Rates	UCF-101	HMDB-51
1	2	94.8	74.1
	4	94.8	74.3
	8	94.5	74.2
	16	94.6	74.2
	2,4	95.1	74.9
2	4,8	95.2	73.7
	8,16	95.2	74.8
	2,8	95.3	73.9
	4,16	95.2	74.5
	2,16	95.1	73.9
3	2,4,8	94.6	74.2
	4,8,16	94.3	74.1
	2, 4, 16	94.1	74.2
<b>4</b>	<b>2, 4, 8, 16</b>	<b>95.9</b>	<b>76.3</b>

VidPrism-C, while the model based on VideoMAE is called VidPrism-M. On HMDB-51, our VidPrism-C model establishes new state-of-the-art results, achieving accuracies of 64.1%, 67.6%, and 74.1% for  $K=4$ , 8, and 16, respectively. On UCF-101, our VidPrism-M variant achieves a clean sweep, setting new state-of-the-art results in all few-shot scenarios and peaking at 96.6% for  $K=16$ . The model further pushes the performance boundary on the SSv2 dataset, reaching 13.6% for  $K=8$  and a new record of 18.3% for  $K=16$ . These results span multiple datasets and  $K$ -shot settings, demonstrating the adaptability of our framework.

Table 4. Effect of Different Supervision.

Type	UCF-101	HMDB-51
$\mathcal{L}_{\text{cls}}$	94.5	75.1
$\mathcal{L}_{\text{cls}} + \mathcal{L}_{\text{rank}}$	95.2	75.6
$\mathcal{L}_{\text{cls}} + \mathcal{L}_{\text{rank}} + \mathcal{L}_{\text{div}}$	95.4	75.5
$\mathcal{L}_{\text{cls}} + \mathcal{L}_{\text{rank}} + \mathcal{L}_{\text{div}} + \mathcal{L}_{\text{gate}}$	<b>95.9</b>	<b>76.3</b>

### 4.3. Ablation Studies

To evaluate the effectiveness of our proposed individual modules, we execute detailed ablation experiments on UCF101 and HMDB51. Unless otherwise stated, all experiments in this section use CLIP ViT-B/16 as the backbone network with 32 input frames. In tables, default settings are in gray, best results are in bold.

**Varying Number of Experts.** We investigate the impact of varying the number of experts and their corresponding time-rate configurations, as shown in Table 3. Starting with a single expert as the baseline, akin to a single-path model, we achieve 94.8% accuracy on UCF-101 and 74.3% on HMDB-51, highlighting the effectiveness yet limitations of a single timescale. Increasing the number of experts to two allowed modeling of two time scales, improving performance; for instance, the rate combination 2, 8 reached 95.3% on UCF-101. However, using three experts cause a slight performance drop, suggesting that more experts alone can introduce redundancy or optimization challenges. The best performance, 95.9% on UCF-101 and 76.3% on HMDB-51, is achieved with four experts covering rates 2, 4, 8, 16, demonstrating the value of diverse temporal res-

Table 5. Ablation studies on the three modules of VidPrism.

Type	UCF-101	HMDB-51	Type	UCF-101	HMDB-51	Type	UCF-101	HMDB-51
Hard Sampling	94.7	75.0	None	95.3	74.2	Avg Pooling	94.8	75.6
Avg Pooling	95.1	75.2	Slow2Fast	95.2	73.6	Linear	94.5	73.9
Max Pooling	95.2	75.5	Fast2Slow	95.0	74.9	MLP	94.7	74.1
<b>RgSTA</b>	<b>95.9</b>	<b>76.3</b>	<b>DBI</b>	<b>95.9</b>	<b>76.3</b>	LocalAttn	95.1	74.6
						<b>GlobalAttn</b>	<b>95.9</b>	<b>76.3</b>

(a) Aggration

(b) Interaction

(c) Combination

olutions. Based on these results, we select this four-expert configuration for our final model.

**Different Aggregation Strategies.** We briefly try four different methods for feature aggregation at different time resolutions, as shown in Table 5a. In addition to the original STAM, we have also selected direct sampling, average pooling, and max pooling. STAM perform best among several methods, demonstrating that the module can better extract information from the input video stream.

**Direction of Interaction.** In addition to the bidirectional interaction (Double), we test three additional functional interaction modules. As shown in Table 5c, ‘None’ indicates that this module is not used, whereas ‘Slow2Fast’ and ‘Fast2Slow’ specify a unidirectional fusion from the slow to the fast pathway and from the fast to the slow pathway, respectively. The results demonstrate that the bidirectional interaction mechanism achieves the best performance among the evaluated methods. In contrast, unidirectional interaction limits the comprehensiveness of the features and can be detrimental to the final representation.

**Combination Strategies.** In Table 5c, we compare five combination methods, ranging from simple functions (Avg Pooling, Linear, MLP) to attention mechanisms. While Local Attention processes each expert’s output in isolation, Global Attention captures dependencies across all experts. The results confirm that GlobalAttn is the superior approach, achieving state-of-the-art accuracies of 95.9% on UCF101 and 76.3% on HMDB51. This highlights the critical need to model global, long-range relationships for effective feature fusion, a capability that localized or context-agnostic methods lack.

**Effect of Different Supervision.** We conduct ablation experiments in Table 4 to evaluate the contributions of each component in the supervision strategy. Starting from the baseline using only cross-entropy (CE) loss, adding ranking loss result in improvements of 0.7% and 0.5% on UCF-101 and HMDB-51, respectively. Further addition of diversity loss continuously improve model performance by promoting functional differentiation among experts. Finally, the introduction of gating loss yield the most significant gain, enabling the complete model to achieve 95.9% and 76.3% accuracy on UCF-101 and HMDB-51, respectively. These results demonstrate the necessity of each supervision module and showcase their synergistic effect.

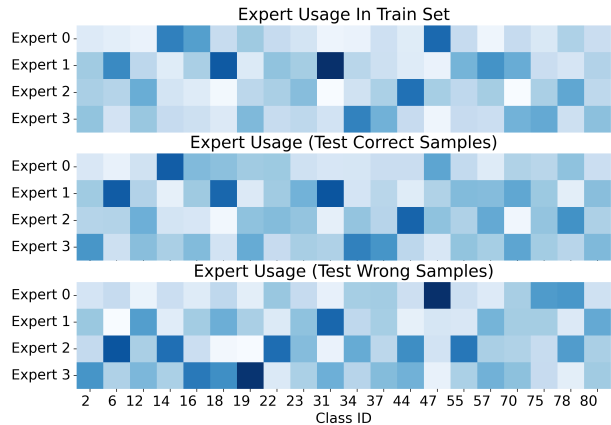


Figure 4. Visualization of Expert Usage on Training and Test Sets.

#### 4.4. Visualization

We visualise expert usage on the UCF-101 dataset in Figure 4, separately aggregating training samples, correctly classified test samples, and misclassified samples. The activation patterns of the training set and correctly classified samples are highly consistent, indicating that the model learns a stable and generalisable expert assignment strategy; moreover, different action categories exhibit distinct expert usage, evidencing a clear functional division of labour among heterogeneous experts rather than redundant, interchangeable units. In contrast, the heatmaps of misclassified samples deviate markedly from these patterns, for example, errors in category 16 are associated with over-activation of expert 3, suggesting that incorrect predictions often arise when model fails to choose the most appropriate expert.

#### 5. Conclusion

In this paper, we introduce VidPrism, a novel heterogeneous temporal Mixture-of-Experts framework designed to advance image-to-video transfer learning. We address the limitation of expert homogenization in conventional MoE models by pioneering a functional division of labor. Through a content-aware, multi-rate sampling module, we provide specialized data streams to experts dedicated to distinct functions. A dynamic, bidirectional fusion mechanism enriches these specialized representations. Extensive experiments demonstrate that VidPrism not only achieves state-of-the-art performance on major video recognition benchmarks but also effectively fosters expert specialization.

## 6. Acknowledgment

This work was supported in part by the National Natural Science Foundation of China under Grant U24B20176 and 62406038.

## References

- [1] Anurag Arnab, Mostafa Dehghani, Georg Heigold, Chen Sun, Mario Lučić, and Cordelia Schmid. Vivit: A video vision transformer. In *ICCV*, pages 6836–6846, 2021. 2
- [2] Jimmy Lei Ba, Jamie Ryan Kiros, and Geoffrey E Hinton. Layer normalization. *arXiv:1607.06450*, 2016. 3
- [3] Andreas Bär, Neil Houlsby, Mostafa Dehghani, and Manoj Kumar. Frozen feature augmentation for few-shot image classification. In *CVPR*, pages 16046–16057, 2024. 1
- [4] Gedas Bertasius, Heng Wang, and Lorenzo Torresani. Is space-time attention all you need for video understanding? In *ICML*, page 4, 2021. 2
- [5] Joao Carreira and Andrew Zisserman. Quo vadis, action recognition? a new model and the kinetics dataset. In *CVPR*, pages 6299–6308, 2017. 2, 6
- [6] Haoxing Chen, Zizheng Huang, Yan Hong, Yanshuo Wang, Zhongcai Lyu, Zhuoer Xu, Jun Lan, and Zhangxuan Gu. Efficient transfer learning for video-language foundation models. In *CVPR*, pages 29129–29138, 2025. 1, 2, 6, 7
- [7] Tongjia Chen, Hongshan Yu, Zhengeng Yang, Zechuan Li, Wei Sun, and Chen Chen. Ost: Refining text knowledge with optimal spatio-temporal descriptor for general video recognition. In *CVPR*, pages 18888–18898, 2024. 6, 7
- [8] Haoqi Fan, Bo Xiong, Karttikeya Mangalam, Yanghao Li, Zhicheng Yan, Jitendra Malik, and Christoph Feichtenhofer. Multiscale vision transformers. In *ICCV*, pages 6824–6835, 2021. 2
- [9] Christoph Feichtenhofer, Axel Pinz, and Andrew Zisserman. Convolutional two-stream network fusion for video action recognition. In *CVPR*, pages 1933–1941, 2016. 2
- [10] Christoph Feichtenhofer, Haoqi Fan, Jitendra Malik, and Kaiming He. Slowfast networks for video recognition. In *ICCV*, pages 6202–6211, 2019. 2
- [11] Melvyn A Goodale and A David Milner. Separate visual pathways for perception and action. *Trends in neurosciences*, 15(1):20–25, 1992. 2
- [12] Raghav Goyal, Samira Ebrahimi Kahou, Vincent Michalski, Joanna Materzynska, Susanne Westphal, Heuna Kim, Valentin Haenel, Ingo Fruend, Peter Yianilos, Moritz Mueller-Freitag, et al. The” something something” video database for learning and evaluating visual common sense. In *ICCV*, pages 5842–5850, 2017. 6
- [13] Zhengrui Guo, Conghao Xiong, Jiabo Ma, Qichen Sun, Lishuang Feng, Jinzhuo Wang, and Hao Chen. Focus: Knowledge-enhanced adaptive visual compression for few-shot whole slide image classification. In *CVPR*, pages 15590–15600, 2025. 1
- [14] Rui Hou, Chen Chen, and Mubarak Shah. Tube convolutional neural network (t-cnn) for action detection in videos. In *ICCV*, pages 5822–5831, 2017. 2
- [15] Chen Ju, Tengda Han, Kunhao Zheng, Ya Zhang, and Weidi Xie. Prompting visual-language models for efficient video understanding. In *ECCV*, pages 105–124. Springer, 2022. 7
- [16] Kumara Kahatapitiya and Michael S Ryoo. Coarse-fine networks for temporal activity detection in videos. In *CVPR*, pages 8385–8394, 2021. 2
- [17] H. Kuehne, H. Jhuang, E. Garrote, T. Poggio, and T. Serre. Hmdb: A large video database for human motion recognition. In *ICCV*, pages 2556–2563, 2011. 6
- [18] Ji Lin, Chuang Gan, and Song Han. Tsm: Temporal shift module for efficient video understanding. In *ICCV*, pages 7083–7093, 2019. 2
- [19] Ziyi Lin, Shijie Geng, Renrui Zhang, Peng Gao, Gerard De Melo, Xiaogang Wang, Jifeng Dai, Yu Qiao, and Hongsheng Li. Frozen clip models are efficient video learners. In *ECCV*, pages 388–404. Springer, 2022. 2
- [20] Ruyang Liu, Jingjia Huang, Ge Li, Jiashi Feng, Xinglong Wu, and Thomas H Li. Revisiting temporal modeling for clip-based image-to-video knowledge transferring. In *CVPR*, pages 6555–6564, 2023. 6
- [21] Ze Liu, Jia Ning, Yue Cao, Yixuan Wei, Zheng Zhang, Stephen Lin, and Han Hu. Video swin transformer. In *CVPR*, pages 3202–3211, 2022. 2
- [22] Muhammad Maaz, Hanoona Rasheed, Salman Khan, and Fahad Khan. Videogpt+: Integrating image and video encoders for enhanced video understanding. *arXiv:2406.09418*, 2024. 2
- [23] Bolin Ni, Houwen Peng, Minghao Chen, Songyang Zhang, Gaofeng Meng, Jianlong Fu, Shiming Xiang, and Haibin Ling. Expanding language-image pretrained models for general video recognition. In *ECCV*, pages 1–18. Springer, 2022. 1, 2, 6, 7
- [24] Junting Pan, Ziyi Lin, Xiatian Zhu, Jing Shao, and Hongsheng Li. St-adapter: Parameter-efficient image-to-video transfer learning. *NeurIPS*, 35:26462–26477, 2022. 2, 6
- [25] Jungin Park, Jiyoung Lee, and Kwanghoon Sohn. Dual-path adaptation from image to video transformers. In *CVPR*, pages 2203–2213, 2023. 6
- [26] Alec Radford, Jong Wook Kim, Chris Hallacy, Aditya Ramesh, Gabriel Goh, Sandhini Agarwal, Girish Sastry, Amanda Askell, Pamela Mishkin, Jack Clark, et al. Learning transferable visual models from natural language supervision. In *ICML*, pages 8748–8763. PmLR, 2021. 1, 2, 6, 7
- [27] Hanoona Rasheed, Muhammad Uzair Khattak, Muhammad Maaz, Salman Khan, and Fahad Shahbaz Khan. Fine-tuned clip models are efficient video learners. In *CVPR*, pages 6545–6554, 2023. 7
- [28] Min Shi, Shihao Wang, Chieh-Yun Chen, Jitesh Jain, Kai Wang, Junjun Xiong, Guilin Liu, Zhiding Yu, and Humphrey Shi. Slow-fast architecture for video multi-modal large language models. *arXiv:2504.01328*, 2025. 2
- [29] Karen Simonyan and Andrew Zisserman. Two-stream convolutional networks for action recognition in videos. *NeurIPS*, 27, 2014. 2
- [30] Khurram Soomro, Amir Roshan Zamir, and Mubarak Shah. Ucf101: A dataset of 101 human actions classes from videos in the wild. *arXiv:1212.0402*, 2012. 1, 6

- [31] V Team, Wenyi Hong, Wenmeng Yu, et al. Glm-4.5 v and glm-4.1 v-thinking: Towards versatile multimodal reasoning with scalable reinforcement learning. *arXiv:2507.01006*, 2025. 2
- [32] Du Tran, Heng Wang, Lorenzo Torresani, Jamie Ray, Yann LeCun, and Manohar Paluri. A closer look at spatiotemporal convolutions for action recognition. In *CVPR*, pages 6450–6459, 2018. 2
- [33] Bin Wang, Bojun Wang, Changyi Wan, Guanzhe Huang, Hanpeng Hu, Haonan Jia, Hao Nie, Mingliang Li, Nuo Chen, Siyu Chen, et al. Step-3 is large yet affordable: Model-system co-design for cost-effective decoding. *arXiv:2507.19427*, 2025. 2
- [34] Heng Wang and Cordelia Schmid. Action recognition with improved trajectories. In *ICCV*, pages 3551–3558, 2013. 2
- [35] Haibo Wang, Zhiyang Xu, Yu Cheng, Shizhe Diao, Yufan Zhou, Yixin Cao, Qifan Wang, Weifeng Ge, and Lifu Huang. Grounded-videollm: Sharpening fine-grained temporal grounding in video large language models. *arXiv:2410.03290*, 2024. 2
- [36] Limin Wang, Yuanjun Xiong, Zhe Wang, Yu Qiao, Dahua Lin, Xiaoou Tang, and Luc Van Gool. Temporal segment networks: Towards good practices for deep action recognition. In *ECCV*, pages 20–36. Springer, 2016. 2
- [37] Limin Wang, Bingkun Huang, Zhiyu Zhao, Zhan Tong, Yinan He, Yi Wang, Yali Wang, and Yu Qiao. Videomae v2: Scaling video masked autoencoders with dual masking. In *CVPR*, pages 14549–14560, 2023. 7
- [38] Mengmeng Wang, Jiazheng Xing, and Yong Liu. Actionclip: A new paradigm for video action recognition. *arXiv:2109.08472*, 2021. 2, 6, 7
- [39] Mengmeng Wang, Jiazheng Xing, Boyuan Jiang, Jun Chen, Jianbiao Mei, Xingxing Zuo, Guang Dai, Jingdong Wang, and Yong Liu. M2-clip: A multimodal, multi-task adapting framework for video action recognition. *AAAI*, 2024. 6
- [40] Mengmeng Wang, Zeyi Huang, Xiangjie Kong, Guojiang Shen, Guang Dai, Jingdong Wang, and Yong Liu. Action detail matters: Refining video recognition with local action queries. In *CVPR*, pages 19132–19142, 2025. 2, 6
- [41] Peng Wang, Yuanzhouhan Cao, Chunhua Shen, Lingqiao Liu, and Heng Tao Shen. Temporal pyramid pooling-based convolutional neural network for action recognition. *IEEE TCSVT*, 27(12):2613–2622, 2016. 2
- [42] Yi Wang, Yinan He, Yizhuo Li, Kunchang Li, Jiashuo Yu, Xin Ma, Xinhao Li, Guo Chen, Xinyuan Chen, Yaohui Wang, et al. Internvid: A large-scale video-text dataset for multimodal understanding and generation. *ICLR*, 2023. 1, 2, 7
- [43] Yi Wang, Xinhao Li, Ziang Yan, Yinan He, Jiashuo Yu, Xiangyu Zeng, Chenting Wang, Changlian Ma, Haian Huang, Jianfei Gao, et al. Internvideo2. 5: Empowering video mllms with long and rich context modeling. *arXiv:2501.12386*, 2025. 2
- [44] Syed Talal Wasim, Muzammal Naseer, Salman Khan, Fahad Shahbaz Khan, and Mubarak Shah. Vita-clip: Video and text adaptive clip via multimodal prompting. In *CVPR*, pages 23034–23044, 2023. 6
- [45] Wenhao Wu, Zhun Sun, and Wanli Ouyang. Revisiting classifier: Transferring vision-language models for video recognition. In *AAAI*, pages 2847–2855, 2023. 1, 6
- [46] Hu Xu, Gargi Ghosh, Po-Yao Huang, Dmytro Okhonko, Armen Aghajanyan, Florian Metzke, Luke Zettlemoyer, and Christoph Feichtenhofer. Videoclip: Contrastive pre-training for zero-shot video-text understanding. In *EMNLP*, 2021. 1, 2
- [47] Mingze Xu, Mingfei Gao, Zhe Gan, Hong-You Chen, Zhengfeng Lai, Haiming Gang, Kai Kang, and Afshin Dehghan. Slowfast-llava: A strong training-free baseline for video large language models. *arXiv:2407.15841*, 2024. 2
- [48] Mingze Xu, Mingfei Gao, Shiyu Li, Jiasen Lu, Zhe Gan, Zhengfeng Lai, Meng Cao, Kai Kang, Yinfei Yang, and Afshin Dehghan. Slowfast-llava-1.5: A family of token-efficient video large language models for long-form video understanding. *arXiv:2503.18943*, 2025. 2
- [49] Ruijia Xu, Guanbin Li, Jihan Yang, and Liang Lin. Larger norm more transferable: An adaptive feature norm approach for unsupervised domain adaptation. In *ICCV*, pages 1426–1435, 2019. 3
- [50] An Yang, Anfeng Li, Baosong Yang, Beichen Zhang, Binyuan Hui, Bo Zheng, Bowen Yu, Chang Gao, Chengen Huang, Chenxu Lv, et al. Qwen3 technical report. *arXiv:2505.09388*, 2025. 2
- [51] Ceyuan Yang, Yinghao Xu, Jianping Shi, Bo Dai, and Bolei Zhou. Temporal pyramid network for action recognition. In *CVPR*, pages 591–600, 2020. 2
- [52] Taojiannan Yang, Yi Zhu, Yusheng Xie, Aston Zhang, Chen Chen, and Mu Li. Aim: Adapting image models for efficient video action recognition. *ICLR*, 2023. 2, 6
- [53] Jianbo Ye, Xin Lu, Zhe Lin, and James Z Wang. Rethinking the smaller-norm-less-informative assumption in channel pruning of convolution layers. *ICLR*, 2018. 3
- [54] Minghao Zhu, Zhengpu Wang, Mengxian Hu, Ronghao Dang, Xiao Lin, Xun Zhou, Chengju Liu, and Qijun Chen. Mote: Reconciling generalization with specialization for visual-language to video knowledge transfer. *NeurIPS*, 37: 55403–55424, 2024. 1, 2, 6, 7